Loss-Gain Equalized Reconfigurable Phaser for Dynamic Radio Analog Signal Processing (R-ASP)

Lianfeng Zou, *Student member, IEEE,* Shulabh Gupta, *member, IEEE,* Christophe Caloz, *Fellow, IEEE*

arXiv:1510.05170v1 [physics.optics] 17 Oct 2015

***Abstract*—We present a loss-gain equalized reconfigurable phaser for dynamic radio analog signal processing (R-ASP). Such a phaser provides real-time tunable group delay response with all-pass transmission. We propose a lumped loss-gain implementation, where tuning and equalization are mostly easily achieved. A theoretical study derives the transfer function and the fundamental characteristics of the device. The phaser is finally experimentally demonstrated, first using a single loss-gain pair and finally a three cascaded loss-gain pair structure with full reconfigurability , where up-chirp and down-chirp group delays are shown for illustration. It is expected that this phaser will find wide applications in radio analog signal processing (R-ASP) systems requiring dynamic adaptability.**

***Index Terms*—Loss-gain pair, equalized phaser, all-pass system, group delay, dispersion engineering, C-section, radio analog signal processing (R-ASP).**

I. Introduction

Radio-analog signal processing (R-ASP) [1], inspired from optical analog signal processing (O-ASP) [2], [3], might be a complementary, if not a substitutive, solution to future millimeter wave and terahertz technology, where conventional digital signal processing is challenging or inapplicable. Reported R-ASP applications include CRLH compressive receiving [4], real-time spectrum analysis [5], real-time spectrogram analysis [6], temporal expansion for enhanced sampling [7], [8], temporal compression and reversal [9], real-time spectrum sniffing [10], SNR enhanced impulse radio transceiving [11], dispersion code multiple access (DCMA) [12], dispersion-based radio-frequency identification [13], [14], scanning rate uniformization in antenna arrays [15], to name a few.

The core of a R-ASP system is a phaser, a device that provides prescribed group delay frequency responses, $\tau(\omega)$, varying from application to application [1], [16]. For instance, linear group delay is used in real-time Fourier transformation [5], [17], stepped group delay is ideal for distortionless frequency discrimination [10], Chebyshev group delay has been used to dispersion-encode radio channels in multiple access communications [12], and a special convex group delay has been synthesized for uniform scanning in an antenna array [15]. Moreover, the group delay swing, $\Delta\tau = \tau_{\max} - \tau_{\min}$, is a crucial parameter in R-ASP. In applications such as real-time Fourier transforming [5], [17] and spectrum sniffing [10], larger $\Delta\tau$ provide better frequency discrimination in time, while in DCMA [12], increasing $\Delta\tau$ results in reduced multi-channel interference, and hence lower bit error rate.

Applications requiring real-time adaptation to dynamic environments would typically require group delay reconfigurability, i.e real-time tunable group delay response ($\tau(\omega)$) or group delay swing ($\Delta\tau$) in R-ASP. One example of such applications is DCMA [12], where the communication channels are essentially time-variant, and hence dynamic communication switching between different pairs of users require real-time reconfiguration of the dispersion codes assigned to each user. In [18], it is shown that, in a single fiber ring resonator [19], varying the loss of the ring results in group delay tuning, where higher loss results in higher group delay swing. However, loss also introduces a notch in the transmission amplitude at the resonance frequency. Moreover, the optical ring resonator in [18] requires a forward-wave (co-directional) coupler, which would be excessively long, and hence not practical, at microwave frequencies [20]. A microwave reconfigurable phaser is reported in [21] using a distributed amplifier to mimic an EBG structure [5], [22], but the obtained amplitude response is strongly frequency dependent, which is generally undesirable in R-ASP since this induces distortion [1]. In [23], an amplification feedback loop is added to a C-section phaser to increase the group delay swing. However, the group delay enhancement there is due to the equivalent cascade of N identical phasers, where N is the iteration counts controlled by an SPDT RF switch, which requires external synchronization and design complication. In that system, the amplification in the feedback loop does not contribute to group delay enhancement, but only loss compensation.

We have shown that introducing balanced loss and gain in a conventional C-section phaser [24]–[26] equally enhances the overall group delay of the phaser while reversing its magnitude response [27]. Furthermore, using equalized loss-gain pair of C-sections results in a perfect phaser, exhibiting flat (all-pass) magnitude and controllable group delay, a response that is impossible in purely passive phasers, where higher group delays are always accompanied with higher loss due to longer time wave trapping, and hence increased dissipation, within the structure. This paper will analytically and experimentally demonstrates the proposed loss-gain pair equalized phasers.

The paper is organized as follows. Section II analyzes separate loss or gain C-sections, first with distributed and then with lumped loss or gain. Section III subsequently presents a combined loss-gain pair phaser. Then Sec. IV and Sec. V describe the design of an equalized loss-gain pair and the experimental demonstration of the resulting all-pass reconfigurable phaser. Finally, a short conclusion is given in Sec. VI.

L. Zou, S. Gupta and C. Caloz are with the Department of Electrical Engineering and Poly-Grames research center, École Polytechnique de Montréal, Montréal, Québec, H3T 1J4, Canada (e-mail: lianfeng.zou@polymtl.ca). C. Caloz is also with King Abdulaziz University, Jeddah, Saudi Arabia (email: christophe.caloz@polymtl.ca).

II. Separate loss or gain C-sections

A. Distributed Loss or Gain C-Sections

A C-section phaser is formed by shorting the end of a backward-wave (contra-directional) coupler, with isolated transmission line propagation constant $\gamma = \beta - j\alpha$ [1]. C-section phasers reported to date are composed of purely *passive* transmission lines, and therefore $\alpha > 0$[1]. We will consider here also *active* transmission line C-section phasers, for which $\alpha < 0$. Such structures might be engineerable using traveling-wave tube structures or active artificial transmission lines. Figure 1 shows the general concept of a gain or loss C-section phaser.

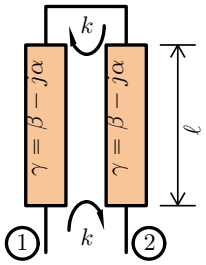

Fig. 1: C-section with physical length ℓ, maximum coupling coefficient k, and isolated transmission line propagation constant $\gamma = \beta - j\alpha$.

The transfer function of such a C-section structure takes the general form [26]

$$\begin{aligned} S_{21} =& \frac{1 - j\kappa \tan\gamma\ell}{1 + j\kappa \tan\gamma\ell} \\ =& \frac{1 - \kappa\tanh\alpha\ell - j(\kappa - \tanh\alpha\ell)\tan\beta\ell}{1 + \kappa\tanh\alpha\ell + j(\kappa + \tanh\alpha\ell)\tan\beta\ell}, \end{aligned} \tag{1}$$

where $\kappa = \sqrt{(1-k)/(1+k)}$, corresponding to the amplitude and the phase

$$|S_{21}| = \sqrt{\frac{(1 - \kappa\tanh\alpha\ell)^2 + (\kappa - \tanh\alpha\ell)^2\tan^2\beta\ell}{(1 + \kappa\tanh\alpha\ell)^2 + (\kappa + \tanh\alpha\ell)^2\tan^2\beta\ell}}, \tag{2a}$$

$$\begin{aligned} \angle S_{21} =& -\arctan\left(\frac{\kappa - \tanh\alpha\ell}{1 - \kappa\tanh\alpha\ell}\tan\beta\ell\right) \\ & -\arctan\left(\frac{\kappa + \tanh\alpha\ell}{1 + \kappa\tanh\alpha\ell}\tan\beta\ell\right), \end{aligned} \tag{2b}$$

respectively. Inspecting (2a) and (2b) reveals that reversing the sign of α reverses $|S_{21}|$ and keeps ϕ_{21} unchanged, i.e.

$$|S_{21}(-\alpha)| = \frac{1}{|S_{21}(\alpha)|}, \tag{3a}$$

$$\angle S_{21}(-\alpha) = \angle S_{21}(\alpha), \tag{3b}$$

respectively. Equations (3a) and (3b) state that equalized distributed loss ($|\alpha|$) and gain ($-|\alpha|$) yields 0 dB-symmetric amplitudes, $20\log(|S_{21}(-\alpha)|) = -20\log(|S_{21}(\alpha)|)$, and identical group delays, $\tau_{21}(-\alpha) = \tau_{21}(\alpha)$, from $\tau_{21} = -\partial\angle S_{21}/\partial\omega$, as plotted in Fig. 2. The tuning effect of distributed loss and gain on group delay will be later shown to allow real-time dispersion engineering. However, *distributed* loss and gain profiles would be difficult to engineer, and we therefore now turn to *lumped* loss and gain inclusions, where the same conclusions will be shown to hold.

[1]The time dependence $e^{+j\omega t}$ is assumed throughout the paper.

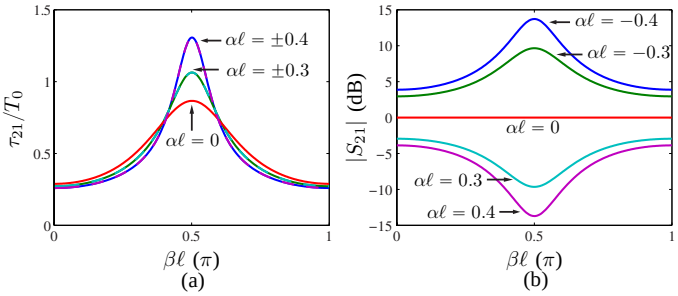

Fig. 2: (a) Normalized group delays, with respect to the period, T_0, of the quarter wavelength frequency and (b) amplitudes, with varying $\alpha\ell$ of a distributed loss or gain C-section, where the coupling factor $k = 0.5$.

B. Lumped Loss or Gain C-Sections

We thus now consider the lumped loss or gain C-section phaser shown in Fig. 3, where the coupler is assumed, in first approximation, to be lossless and terminated at one end by a load. The coupler lossless approximation is very reasonable since dispersion loss is typically much larger than transmission line conductive or dielectric losses [1]. Assuming perfect load

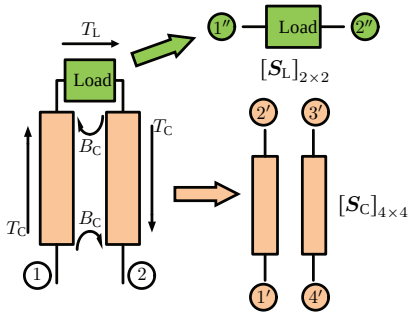

Fig. 3: Loaded C-section consisting of a coupled-line coupler, represented by a 4×4 scattering matrix, $[S_{\rm C}]_{4\times4}$, and a load represented by a 2×2 scattering matrix, $[S_{\rm L}]_{2\times2}$.

matching, the scattering matrix of the load is

$$[\boldsymbol{S}_{\rm load}]_{2\times2} = \begin{bmatrix} 0 & T_{\rm L} \\ T_{\rm L} & 0 \end{bmatrix}, \tag{4a}$$

where

$$T_{\rm L}(\omega) = A_{\rm L}(\omega)e^{j\phi_{\rm L}(\omega)}, \tag{4b}$$

is the load transfer function. Further assuming coupler perfect matching and isolation, the scattering matrix of the coupler is

$$[\boldsymbol{S}_{\rm C}]_{4\times4} = \begin{bmatrix} 0 & T_{\rm C} & 0 & B_{\rm C} \\ T_{\rm C} & 0 & B_{\rm C} & 0 \\ 0 & B_{\rm C} & 0 & T_{\rm C} \\ B_{\rm C} & 0 & T_{\rm C} & 0 \end{bmatrix}, \tag{5a}$$

where

$$B_{\rm C}(\omega) = \frac{jk\sin\theta}{\sqrt{1-k^2}\cos\theta + j\sin\theta}, \tag{5b}$$

$$T_{\rm C}(\omega)=\frac{\sqrt{1-k^2}}{\sqrt{1-k^2}\cos\theta+j\sin\theta}, \tag{5c}$$

are the backward coupling and through transfer functions, respectively [20], with parameters k and $\theta=\pi\omega/2\omega_0$ being the maximum coupling, occurring at the quarter-wavelength frequency ω_0, and the electrical length of the coupler at that frequency, respectively.

The backward coupling introduces a feedback loop from the load output port $2''$ to the load input port $1''$ (see Fig. 3), leading to multiple scattering at port 2 of the loaded C-section. Assuming unity excitation to the loaded C-section port 1 and accounting for the multiple scattering events, one finds

$$\begin{aligned}S_{21}=&S_{12}\\ =&B_{\rm C}+T_cT_{\rm L}T_{\rm C}+T_{\rm C}T_{\rm L}B_{\rm C}T_{\rm L}T_{\rm C}\\ &+T_{\rm C}T_{\rm L}B_{\rm C}T_{\rm L}B_{\rm C}T_{\rm L}T_{\rm C}+\ldots\\ =&B_{\rm C}+T_{\rm C}^2T_{\rm L}\sum_{n=0}^{\infty}(B_{\rm C}T_{\rm L})^n.\end{aligned} \tag{6}$$

If $|B_{\rm C}T_{\rm L}|\geqslant 1$, the geometric series (6) diverges, corresponding to an oscillatory (unstable) regime. Therefore, the condition $|B_{\rm C}T_{\rm L}|<1$ must be enforced for stability, in which case (6) reduces to

$$S_{21}=S_{12}=B_{\rm C}+\frac{T_{\rm C}^2T_{\rm L}}{1-B_{\rm C}T_{\rm L}}, \tag{7}$$

with

$$|T_{\rm L}(\omega)|=A_{\rm L}(\omega)<\frac{1}{|B_{\rm C}(\omega)|}. \tag{8}$$

Moreover, according to [28], the maximum of the group delay occurs at the resonance frequency, $\omega_{\rm p}$, where the multiple scattered waves add in phase. This is equivalent to the following phase condition

$$\angle[T_{\rm L}(\omega_{\rm p})B_{\rm C}(\omega_{\rm p})]=\phi_{\rm L}(\omega_{\rm p})+\angle B_{\rm C}(\omega_{\rm p})=2n\pi, \tag{9}$$

where n is an integer. Equation (9) suggests that, given a coupler with known $\angle B_c(\omega)$, the resonance frequency, $\omega_{\rm p}$, may be tuned by varying the load transmission phase $\phi_{\rm L}$.

Inserting (4b), (5b) and (5c) into (6) yields

$$\begin{aligned}S_{21}=&T_{\rm L}\frac{\sqrt{1-k^2}\cot\theta+k/A_{\rm L}\sin\phi_{\rm L}-j\left(1-k/A_{\rm L}\cos\phi_{\rm L}\right)}{\sqrt{1-k^2}\cot\theta+kA_{\rm L}\sin\phi_{\rm L}+j\left(1-kA_{\rm L}\cos\phi_{\rm L}\right)}\\ =&|S_{21}|\,e^{j\phi_{21}},\end{aligned} \tag{10a}$$

where

$$|S_{21}|=A_{\rm L}\sqrt{\frac{\left(\sqrt{1-k^2}\cot\theta+k/A_{\rm L}\sin\phi_{\rm L}\right)^2+\left(1-k/A_{\rm L}\cos\phi_{\rm L}\right)^2}{\left(\sqrt{1-k^2}\cot\theta+kA_{\rm L}\sin\phi_{\rm L}\right)^2+\left(1-kA_{\rm L}\cos\phi_{\rm L}\right)^2}}, \tag{10b}$$

$$\begin{aligned}\angle S_{21}=&-\arctan\frac{1-k/A_{\rm L}\cos\phi_{\rm L}}{\sqrt{1-k^2}\cot\theta+k/A_{\rm L}\sin\phi_{\rm L}}\\ &-\arctan\frac{1-kA_{\rm L}\cos\phi_{\rm L}}{\sqrt{1-k^2}\cot\theta+kA_{\rm L}\sin\phi_{\rm L}}\\ &+\phi_{\rm L},\end{aligned} \tag{10c}$$

Inspecting (10b) and (10c) reveals that reversing the load transmission amplitude, i.e. $A_{\rm L}\rightarrow 1/A_{\rm L}$, reverses the loaded C-section transfer function amplitude, $|S_{21}|$, while keeping the transmission phase $\angle S_{21}$, and hence also the group delay, τ_{21}, unchanged. Therefore, the lumped loss or gain loaded C-section indeed exhibits the same fundamental properties as its distributed counterpart. For simplicity, we next assume that the load transmission is of constant amplitude and linear phase, or is non-dispersive, i.e. $A_{\rm L}(\omega)=G(G>1)$ or $A_{\rm L}(\omega)=L(L<1)$, so that

$$\phi_{\rm L}=-\tau_{\rm L}\omega, \tag{11}$$

where $\tau_{\rm L}$ is the load transmission delay. we may now parametrically study the behavior of the loaded C-section. Assuming the first resonance frequency, $\omega_{\rm p}=\omega_0$, the maximum of the loaded C-section group delay corresponds then to

$$\begin{aligned}\tau_{21}^{\max}(A_{\rm L},\omega)=&\tau_{21}(A_{\rm L},\omega_0)=-\left.\frac{\partial\phi_{21}}{\partial\omega}\right|_{\omega=\omega_0}\\ =&\frac{T_0\sqrt{1-k^2}}{4}\left(\frac{1}{1-k/A_{\rm L}}+\frac{1}{1-kA_{\rm L}}\right)\\ &+\tau_{\rm L}k\left(\frac{1/A_{\rm L}}{1-k/A_{\rm L}}+\frac{A_{\rm L}}{1-kA_{\rm L}}\right)\\ &+\tau_{\rm L},\end{aligned} \tag{12}$$

where $\phi_{\rm L}(\omega_0)=2n\pi-\angle B_{\rm C}(\omega_0)=2n\pi$, with $\angle B_{\rm C}(\omega_0)=0$ [20] has been used. Further assuming $\tau_{\rm L}=0$ reduces (12) to

$$\tau_{21}^{\max}(A_{\rm L},\omega)=\frac{T_0\sqrt{1-k^2}}{4}\left(\frac{1}{1-k/A_{\rm L}}+\frac{1}{1-kA_{\rm L}}\right), \tag{13}$$

with $T_0=1/f_0$ being the period at the quarter-wavelength frequency. The minimum loaded C-section group delay occurring at the first anti-resonance frequency, $2\omega_{\rm p}=2\omega_0$, is

$$\begin{aligned}\tau_{21}^{\min}(A_{\rm L},\omega)=&\tau_{21}(A_{\rm L},2\omega_0)=-\left.\frac{\partial\phi_{21}}{\partial\omega}\right|_{\omega=2\omega_0,\tau_{\rm L}=0}\\ =&\frac{T_0}{4\sqrt{1-k^2}}\left(2-kA_{\rm L}-\frac{k}{A_{\rm L}}\right),\end{aligned} \tag{14}$$

The difference of the last two relations corresponds to the group delay swing

$$\begin{aligned}\Delta\tau_{21}(A_{\rm L})=&\tau_{21}^{\max}(A_{\rm L},\omega)-\tau_{21}^{\min}(A_{\rm L},\omega)\\ =&\frac{T_0k\left(A_{\rm L}+1/A_{\rm L}-2k\right)}{4\sqrt{1-k^2}}\left(\frac{1}{1-k/A_{\rm L}}+\frac{1}{1-kA_{\rm L}}\right).\end{aligned} \tag{15}$$

We may at this point define the loaded C-section transmission group delay swing and amplitude tuning factors

$$\begin{aligned}\sigma_{\Delta\tau}(A_{\rm L})=&\frac{\Delta\tau_{21}(A_{\rm L})}{\Delta\tau_{21}(A_{\rm L}=1)}\\ =&\frac{A_{\rm L}+1/A_{\rm L}-2k}{4}\left(\frac{1}{1-k/A_{\rm L}}+\frac{1}{1-kA_{\rm L}}\right)\end{aligned} \tag{16a}$$

and

$$\sigma_A(A_{\rm L}) = \frac{|S_{21}(A_{\rm L},\omega_0)|}{|S_{21}(A_{\rm L}=1,\omega_0)|} = |S_{21}(A_{\rm L},\omega_0)| = \left|\frac{A_{\rm L}-k}{1-kA_{\rm L}}\right|. \quad (16b)$$

Figure 4 shows $\sigma_{\Delta\tau}(A_{\rm L})$ and $\sigma_A(A_{\rm L})$ with three different coupling factors k. We see that $\sigma_{\Delta\tau}(A_{\rm L})$ and $\sigma_A(A_{\rm L})$ (in dB) are even and odd function of $A_{\rm L}$ (in dB), respectively, which means that a balanced pair of load loss and load gain have same tuning effect on group delay swing, while opposite tuning effect on amplitude. Moreover, smaller k gives higher group delay swing tuning range but at the cost of using higher loss or gain load and hence consuming more power. Also note that $A_{\rm L}$ going above upper limit $1/k$ leads to oscillation, which should be avoided, while going below lower limit k results in negative group delay, which has been presented in [28].

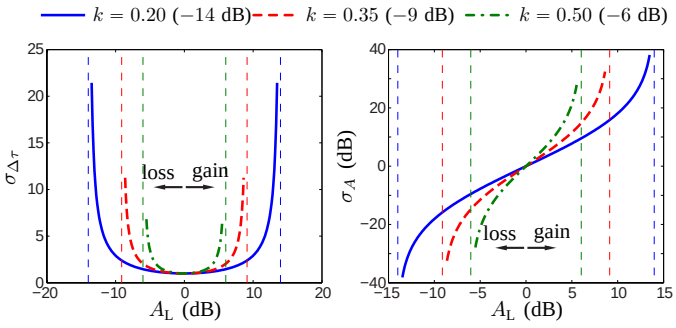

(a) (b)

Fig. 4: Tuning effect of the load transmission amplitude, $A_{\rm L}$ in dB, on (a) the loaded C-section group delay swing and (b) the transmission amplitude, respectively, with tuning range of $A_{\rm L}$ defined by k as the lower limit (left dashed line) and $1/k$ as the upper limit (right dashed line). Range: $A_{\rm L} \in [k + 0.5 \text{ dB}, 1/k - 0.5 \text{ dB}]$.

Figure 5 shows the loaded C-section transmission group delays and amplitudes for coupling coefficient $k = 0.5$. We see that the equalized loss and gain pair exhibits identical group delay and symmetric amplitudes about $|S_{21}| = 0$ dB.

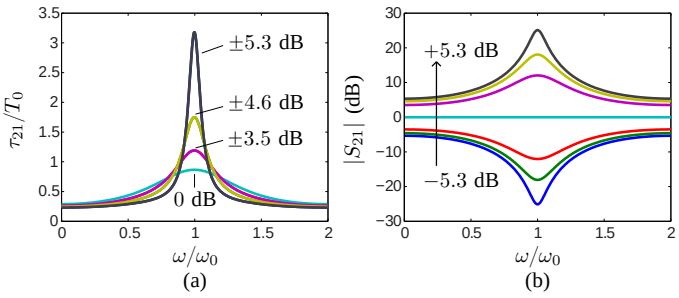

(a) (b)

Fig. 5: Loaded C-section (a) normalized group delays τ_{21}/T_0 and (b) transmission amplitudes $|S_{21}|$, with maximum coupling factor $k = -6$ dB ($k = 0.5$) at ω_0, and varying load transmission amplitudes $A_{\rm L} = \{0, \pm 3.5, \pm 4.6, \pm 5.3\}$ dB.

Apart from tuning the height of group delay peak, the position of group delay peak, $\omega_{\rm p}$, or resonance frequency, can be also tuned by varying the load transmission phase, $\phi_{\rm L}$, as shown in Fig. 6. The value of $\omega_{\rm p}$ is determined by using (9).

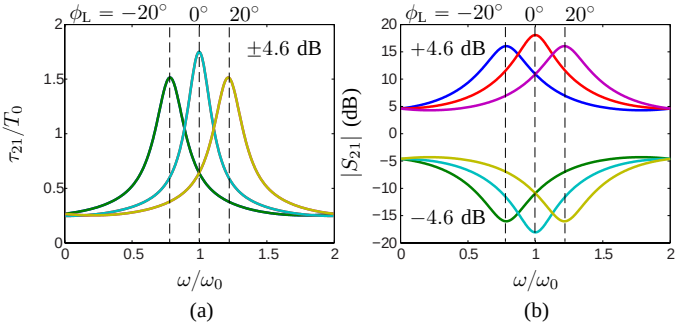

(a) (b)

Fig. 6: Loaded C-section (a) normalized group delays τ_{21}/T_0 and (b) transmission amplitudes $|S_{21}|$, with maximum coupling factor $k = 6$ dB ($k = 0.5$) at ω_0 and $A_{\rm L} = \pm 4.6$ dB, and varying load transmission phase $\phi_{\rm L} = \{-20°, 0°, 20°\}$.

III. Combined Loss-Gain Equalized Pair

An all-pass loss-gain equalized pair is formed by serially connecting a loss C-section and a gain C-section, as shown in Fig. 7, with appropriately tune gain, G, and loss, L, such that $G = 1/L$. The group delay of the resulting loss-gain pair is twice that of a single loss or gain loaded C-section phaser, as shown in Fig. 8(a), while the transmission amplitude becomes all-pass [Fig. 8(b)].

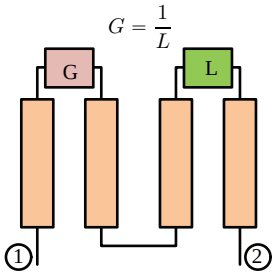

Fig. 7: Proposed all-pass loss-gain equalized pair formed by serially connecting a loss loaded C-section and a gain loaded C-section, where the gain is the reverse of the loss, $G = 1/L$.

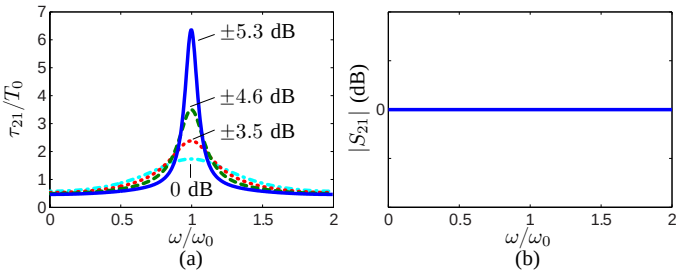

(a) (b)

Fig. 8: Loss-gain equalized pair (a) normalized group delay τ_{21}/T_0 and (b) all-pass transmission amplitude $|S_{21}|$, with maximum coupling factor $k = 0.5$ at ω_0 and different load transmission amplitudes $A_{\rm L} = \{0, \pm 3.5, \pm 4.6, \pm 5.3\}$ dB.

The analysis performed so far assumes an ideal (lossless, perfectly matched and perfectly isolated) system. As a result, the loaded C-section is stable as long as condition (8) is satisfied. In reality, the loaded C-section phaser may still become unstable due to non-ideal factors, such as coupler

forward-wave coupling (imperfect isolation) and load mismatch, since such non-idealities create wave paths that have not been accounted for in (8). A detailed stability analysis of a real C-section phaser is beyond the scope of this paper, and will be presented elsewhere. However, maximizing isolation and matching clearly appears to represent important design considerations from the viewpoint of stability.

IV. Design of Loss-Gain Pair

A. Microstrip Coupler

The C-section phaser is implemented here in microstrip technology for easiest fabrication and testing. Unfortunately, due to their imperfect transverse electromagnetic nature, and corresponding unequal even and odd mode phase velocities ($v_o > v_e$), microstrip couplers suffer from relatively poor isolation [20]. To minimize the aforementioned subsequent risks of instability, one should thus increase the natural isolation of the coupler. Corresponding equalization of even and odd velocities may be achieved by different approaches, such as using wiggly transmission lines [29], inductive compensation [30] or capacitive compensation [31], etc. We use here capacitive compensation, which consists in inserting a coupling enhancing capacitance in the gap between the two transmission lines.

The fabricated microstrip coupler is shown in Fig. 9 while Fig. 10 shows the corresponding measured response, with best matching and isolation reached near 2.5 GHz and corresponding -10 dB coupling. Therefore we will choose operation frequency around 2.5 GHz in the design of phaser later.

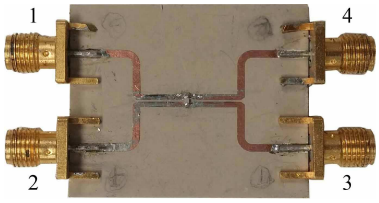

Fig. 9: Fabricated microstrip coupler (Rogers RO6010, $\epsilon_r = 10.2$, 0.5 oz cladding, 50 mil substrate).

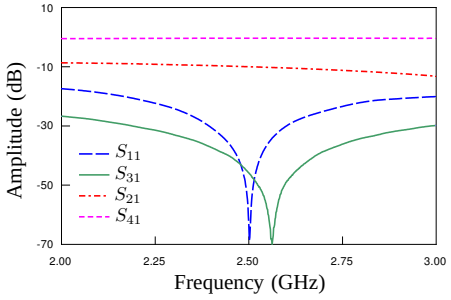

Fig. 10: Measured S-parameters of the microstrip coupler shown in Fig. 9.

B. Variable Loss-Gain Load

The fabricated loss-gain load is shown in Fig. 11 with parts specifications. It is composed of the series connection of an internally matched variable loss-gain (VLG) chip, whose loss-gain is tuned by varying the control bias voltage, and a fixed stabilization and matching enhancement attenuator (ATT). Both the VLG internal matching and the ATT matching and attenuation contribute to the stability of the overall device discussed in Sec. III.

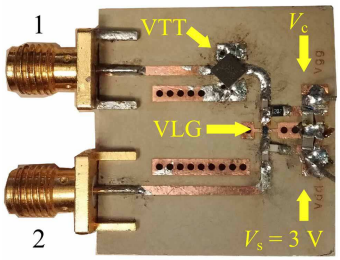

Fig. 11: Fabricated variable loss or gain load (same substrate as in Fig. 9) composed a VLG (Avago VMMK-3503 [32]: internal matching, $0.5-18$ GHz operation, 10 dB gain to 13 dB loss tuning range (23 dB interval) by varying V_c from 1.8 V to 0 V) and a fixed stabilization and matching enhancement attenuator (Minicircuit GAT-4+: 4 dB attenuation).

Figure 10 shows the corresponding measured response. The maximum measured gain is limited by the attenuator to the level of 6.7 dB, which lies in the stability region prescribed by (8), namely $|T_{LF}(2.5\text{ GHz})|^{\max} = 1/|B_c(2.5\text{ GHz})| = 10$ dB.

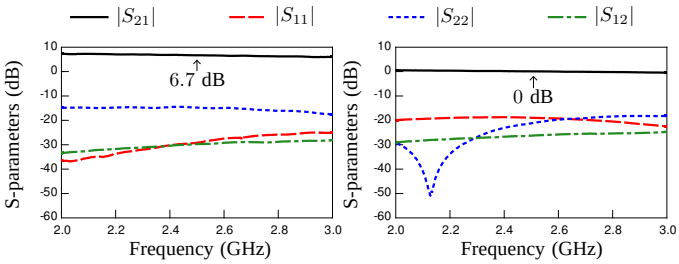

Fig. 12: Measured amplitude responses of the load shown in Fig. 11 for (a) $|T_L(2.5\text{ GHz})| = 6.7$ dB and (b) $|T_L(2.5\text{ GHz}| = 0$ dB.

C. Numerical and Experimental Demonstration of Loss-Gain C-Sections

The performance of the loss or gain C-section phaser may be predicted using a commercial RF circuit simulator by importation of the measured coupler and load responses into two-port and four-port scattering models, respectively. Figure 13(a) shows the corresponding responses. The relatively high reflection $|S_{22}|$ is not a concern, since propagation is from port 1 to port 2, as long as good matching is achieved at port 1 of loaded C-sections (see Fig. 3).

The forward transmission $|S_{21}(2.5\text{ GHz})| \approx 16$ dB, with $|T_L| = 6.7$ dB, corresponding to the enhanced group delay $\tau_{21}(2.5\text{ GHz}) \approx 3$ ns [Fig. 13(b)], while $|S_{21}(2.5\text{ GHz})| \approx 0$ dB, with $|T_L| = 0$ dB, corresponding to conventional C-section (all pass) with group delay

$\tau_{21}(2.5\text{ GHz}) \approx 1.7$ ns. The loss C-section performance is not simulated here because it is less possible to oscillate than gain C-section, but it will be shown later in the experiment.

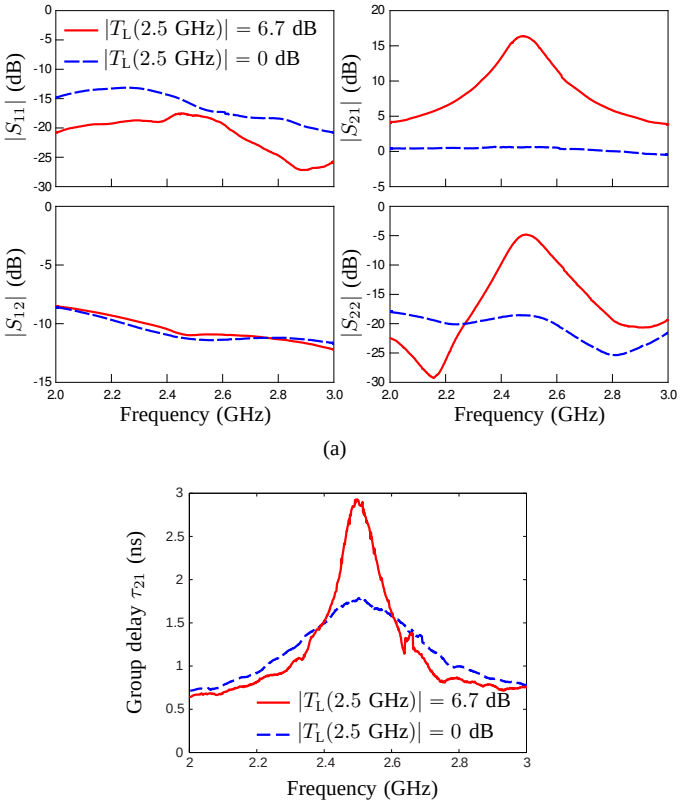

Fig. 13: Simulated (a) amplitudes and (b) group delays of a loaded C-section phasers with imported coupler and load experimental models corresponding to Fig. 10 and Fig. 12, respectively.

Figure 14 shows the fabricated loaded C-section. The corresponding measured amplitudes and group delays, with varied load loss and gain, are plotted in Fig. 15. Consistently with the analysis presented in Sec. II-B, the forward transmission amplitudes are symmetric about 0 dB while the group delays are identical.

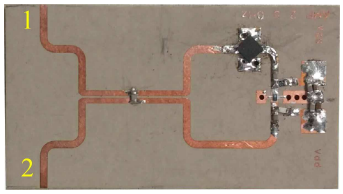

Fig. 14: Fabricated loaded C-section phaser.

Figure 16 shows the fabricated equalized loss-gain pair phaser. The corresponding measured amplitudes and group delays, with varied load loss and gain, are plotted in Fig. 17. Consistently with the analysis presented in Sec. III, the combined pair transmission amplitudes are nearly flat while combined pair group delays are twice of the loss or gain C-section [compare to Fig. 15(b)].

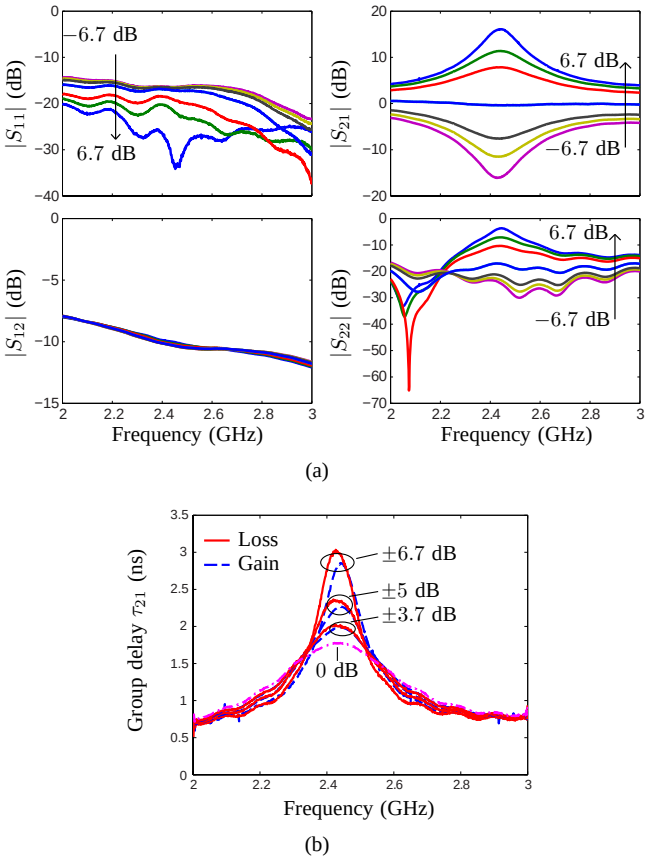

Fig. 15: Measured (a) amplitudes and (b) group delays of the loss or gain C-section in Fig. 14, with varying gains and losses $|T_L| = \{0, \pm 3.7, \pm 5, \pm 6.7\}$ dB.

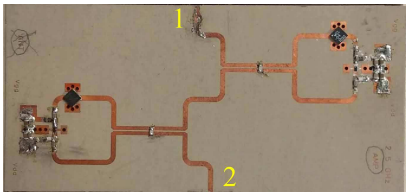

Fig. 16: Fabricated equalized loss-gain pair phaser.

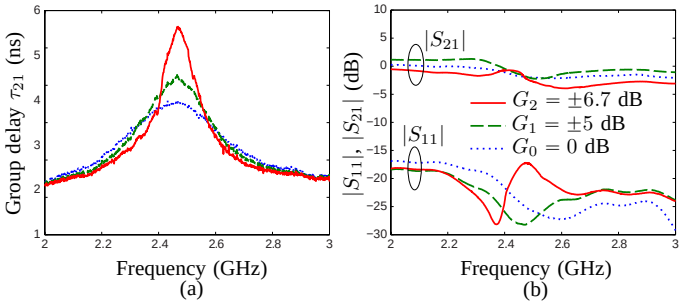

Fig. 17: Measured (a) group delays and (b) amplitudes of the loss-gain pair phaser in Fig. 16.

V. Reconfigurable Cascaded Loss-Gain Pair Phaser

A. Constitutive Loss-Gain Pairs

Cascading loss-gain equalized pairs tuned at different resonance frequencies allows to synthesize reconfigure group delay responses in real time with all-pass amplitude response over a certain bandwidth. To demonstrate this, we fabricated three loss-gain equalized pairs, shown in Fig. 18, tuned at $\omega_{p1} = 2.35$, $\omega_{p2} = 2.45$ and $\omega_{p3} = 2.6$ GHz, respectively.

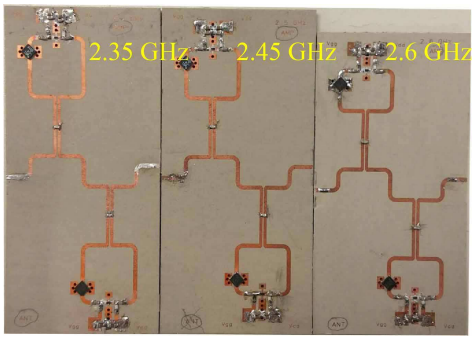

Fig. 18: Fabricated loss-gain equalized pairs, tuned at 2.35, 2.45 and 2.6 GHz, respectively, by varying the length of the loads. The incorporated couplers are all identical.

B. Experimental Results

The experimental setup and complete device under test are shown in Fig. 19(a) and Fig. 19(b), respectively. The 3-section reconfigurable phaser is formed by cascading the three loss-gain equalized pairs, which were clipped on a copper plate placed underneath the pairs. The scattering matrix and group delay were measured on a vector network analyzer. The two power supplies provide a source voltage of $V_s = 3$ V and a control voltage of $V_c = 2$ V, respectively.

In Fig. 20 the control voltages (V_c) of the 3 loss-gain pairs (6 voltages in all) are tuned to produce up-chirp and down-chirp linear group delay responses [1]. This demonstrates the central point of the paper: the group delay response of the phaser can be reconfigured in real time with essentially all-pass transmission. The reconfigurability shown here, between positive and negative chirp responses, is naturally only an illustrative choice, other group delay responses being achievable with this phaser.

VI. Conclusion

A loss-gain equalized reconfigurable phaser has been proposed, analyzed and demonstrated. Experimental results have confirmed that such a device provides real-time group delay reconfigurability while exhibiting an all-pass response. It will enable radio analog signal processing (R-ASP) systems requiring dynamic adaptability, as for instance dispersion code multiple access (DCMA).

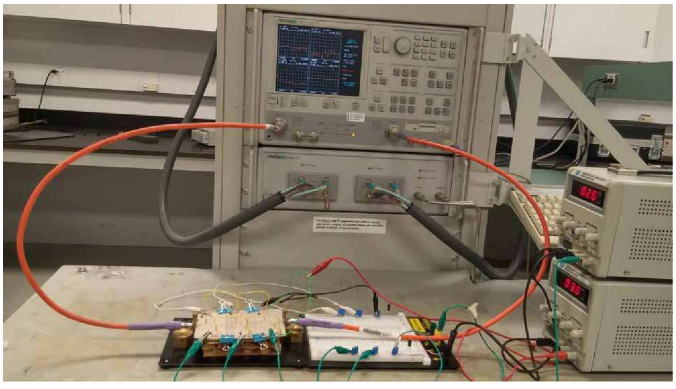

(a)

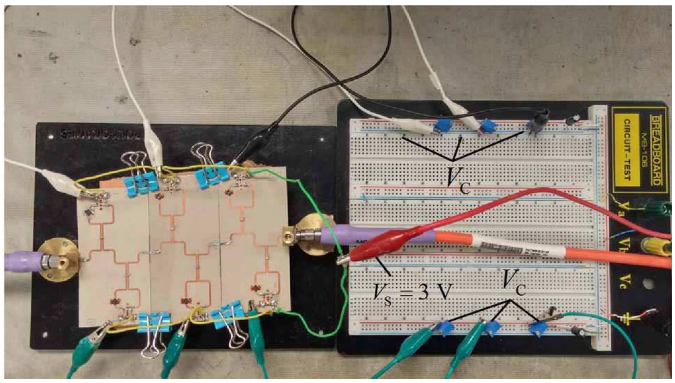

(b)

Fig. 19: (a) Experimental setup and (b) device under test, where a 3-section loss-gain reconfigurable phaser is formed by cascading three loss-gain equalized pairs.

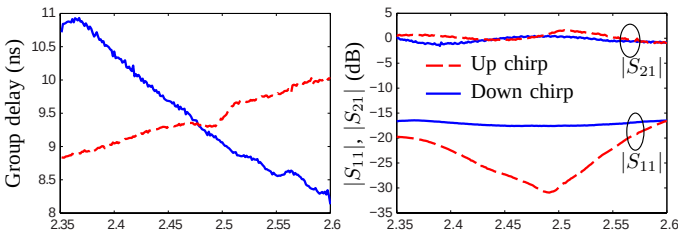

Fig. 20: (a) Group delays and (b) Transmission and reflection amplitudes of the cascade 3-section reconfigurable phaser.

References

[1] C. Caloz, S. Gupta, Q. Zhang, and B. Nikfal, "Analog signal processing: A possible alternative or complement to dominantly digital radio schemes," *IEEE Microw. Mag.*, vol. 14, no. 6, pp. 87–103, Sep. 2013.

[2] B. E. A. Saleh and M. C. Teich, *Fundamentals of Photonics 2nd Ed.* Hoboken, NJ: John Wiley, 2007.

[3] J. Azaña, "Ultrafast analog all-optical signal processors based on fiber-grating devices," *IEEE Photon. J.*, vol. 2, no. 3, pp. 359–386, Jun. 2010.

[4] S. Abielmona, S. Gupta, and C. Caloz, "Compressive receiver using a CRLH-based dispersive delay line for analog signal processing," *IEEE Trans. Microw. Theory Tech.*, vol. 57, no. 11, pp. 2617–2626, Nov. 2009.

[5] M. A. G. Laso, T. Lopetegi, M. J. Erro, D. Benito, M. J. Garde, M. A. Muriel, M. Sorolla, and M. Guglielmi, "Real-time spectrum analysis in microstrip technology," *IEEE Trans. Microw. Theory Tech.*, vol. 51, no. 3, pp. 705–717, Mar. 2003.

[6] S. Gupta, S. Abielmona, and C. Caloz, "Microwave analog real-time spectrum analyzer (RTSA) based on the spectral-spatial decomposition

property of leaky-wave structures," *IEEE Trans. Microw. Theory Tech.*, vol. 57, no. 12, pp. 2989–2999, Dec. 2009.

[7] J. D. Schwartz, J. Azaña, and D. V. Plant, "A fully electronic system for the time magnification of ultra-wideband signals," *IEEE Trans. Microw. Theory Tech.*, vol. 55, no. 2, pp. 327–334, Feb. 2007.

[8] B. Xiang, A. Kopa, Z. Fu, and A. B. Apsel, "Theoretical analysis and practical considerations for the integrated time-stretching system using dispersive delay line (DDL)," *IEEE Transactions on Microwave Theory and Techniques*, vol. 60, no. 11, pp. 3449–3457, Nov. 2012.

[9] J. D. Schwartz, J. Azaña, and D. V. Plant, "An electronic temporal imaging system for compression and reversal of arbitrary UWB waveforms," in *Proc. IEEE Radio and Wireless Symp.*, Orlando, FL. U.S., Jan. 2008, pp. 487–490.

[10] B. Nikfal, D. Badiere, M. Repeta, B. Deforge, S. Gupta, and C. Caloz, "Distortion-less real-time spectrum sniffing based on a stepped group-delay phaser," *IEEE Microw. Wireless Compon. Lett.*, vol. 22, no. 11, pp. 601–603, Nov. 2012.

[11] B. Nikfal, Q. Zhang, and C. Caloz, "Enhanced-SNR impulse radio transceiver based on phasers," *IEEE Microw. Wireless Compon. Lett.*, vol. 24, no. 11, pp. 778–780, Nov. 2014.

[12] S. Gupta, L. Zou, M. A. Salem, and C. Caloz, "Bit-error-rate (BER) performance in dispersion code multiple access (DCMA)," in *Proc. IEEE Int. Symp. on Antennas Propag.*, Vancouver, BC, Canada, Jul. 2015, pp. 1015–1016.

[13] E. Perret, M. Hamdi, G. E. P. Tourtollet, R. Nair, F. Garet, A. Delattre, A. Vena, L. Duvillaret, P. Martinez, S. Tedjini, and Y. Boutant, "THID, the next step of chipless RFID," in *RFID IEEE Intl Conf.*, Penang, Malaysia, Apr. 2013.

[14] S. Gupta, B. Nikfal, and C. Caloz, "Chipless RFID system based on group delay engineered dispersive delay structures," *IEEE Antennas and Wireless Propag. Lett.*, vol. 10, pp. 1366–1368, Oct. 2011.

[15] G. Zhang, Q. Zhang, F. Yang, Y. Chen, C. Caloz, and R. D. Murch, "Phaser-based feeding network for uniformly scanning antenna arrays," in *Proc. IEEE Int. Symp. on Antennas Propag.*, Vancouver, BC, Canada, Jul. 2015, pp. 236–237.

[16] S. Gupta, Q. Zhang, L. Zou, L. Jiang, and C. Caloz, "Generalized coupled-line all-pass phasers," *IEEE Trans. Microw. Theory Tech.*, vol. 63, no. 3, pp. 1–12, Mar. 2015.

[17] M. A. Muriel, J. Azaña, and A. Carballar, "Real-time Fourier transformer based on fiber gratings," *Opt. Lett.*, vol. 24, no. 1, pp. 1–3, Jan. 1999.

[18] O. Schwelb, "Transmission, group delay, and dispersion in single-ring optical resonators and add/drop filters - a tutorial overview," *J. Lightw. Technol.*, vol. 22, no. 5, pp. 1380–1394, May 2004.

[19] K. P. Jackson, S. A. Newton, B. Moslehi, M. T. C. C. Cutler, J. W. Goodman, and H. J. Shaw, "Optical fiber delay-line signal processing," *IEEE Trans. Microw. Theory Tech.*, vol. 33, no. 3, pp. 193–210, Mar. 1985.

[20] R. K. Mongia, I. J. Bahl, P. Bhartia, and J. Hong, *RF and Microwave Coupled-Line Circuits, 2nd Ed.* Norwood, MA: Artech House, 2007.

[21] B. Xiang, X. Wang, and A. B. Apsel, "A reconfigurable integrated dispersive delay line (RI-DDL) in 0.13-μm CMOS process," *IEEE Trans. Microw. Theory Tech.*, vol. 61, no. 7, pp. 2610–2619, Jul. 2013.

[22] I. Arnedo, I. Arregui, M. Chudzik, F. Teberio, A. Lujambio, D. Benito, T. Lopetegi, and M. A. G. Laso, "Direct and exact synthesis: Controlling the microwaves by means of synthesized passive components with smooth profiles," *IEEE Microw. Mag.*, vol. 16, no. 4, pp. 114–128, May 2015.

[23] B. Nikfal, S. Gupta, and C. Caloz, "Increased group delay slope loop system for enhanced-resolution analog signal processing," *IEEE Trans. Microw. Theory Tech.*, vol. 59, no. 6, pp. 1622–1628, Jun. 2011.

[24] E. G. Cristal, "Analysis and exact synthesis of cascaded commensurate transmission-line C-section all-pass networks," *IEEE Trans. Microw. Theory Tech.*, vol. 14, no. 6, pp. 285 – 291, Jun. 1966.

[25] ——, "Theory and design of transmission line all-pass equalizers," *IEEE Trans. Microw. Theory Tech.*, vol. 17, no. 1, pp. 28–38, Jan. 1969.

[26] S. Gupta, A. Parsa, E. Perret, R. V. Snyder, R. J. Wenzel, and C. Caloz, "Group-delay engineered noncommensurate transmission line all-pass network for analog signal processing," *IEEE Trans. Microw. Theory Tech.*, vol. 58, no. 9, pp. 2392–2407, Sep. 2010.

[27] L. Zou, S. Gupta, and C. Caloz, "Reconfigurable phaser using gain-loss C-sections for radio analog signal processing (R-ASP)," in *IEEE Asia Pacific Microw. Conf. (APMC)*, Nanjing, PRC, Dec. 2015, accepted.

[28] Q. Zhang, D. L. Sounas, S. Gupta, and C. Caloz, "Wave interference explanation of group delay dispersion in resonators," *IEEE Antennas Propag. Mag.*, vol. 55, no. 2, pp. 212–227, May 2013.

[29] S. Uysal and H. Aghvami, "Synthesis, design, and construction of ultra-wide-band nonuniform quadrature directional couplers in inhomogeneous media," *IEEE Trans. Microw. Theory Tech.*, vol. 37, no. 6, pp. 969–976, Jun. 1989.

[30] S. Lee and Y. Lee, "A design method for microstrip directional couplers loaded with shunt inductors for directivity enhancement," *IEEE Trans. Microw. Theory Tech.*, vol. 58, no. 4, pp. 994–1002, Apr. 2010.

[31] M. Dydyk, "Microstrip directional couplers with ideal performance via single-element compensation," *IEEE Trans. Microw. Theory Tech.*, vol. 47, no. 6, pp. 956–964, Jun. 1999.

[32] *VMMK-3503* $0.5 - 18$ *GHz Variable Gain Amplifier in SMT Package Data Sheet*, Avago Technologies, Dec. 2012.